Dynamical multi-breakup processes in the ^{124}Sn+^{64}Ni system at 35 MeV/nucleon

M. Papa,[1] F. Amorini,[2] A. Anzalone,[2] L. Auditore,[3] V. Baran,[4] I. Berceanu,[4] J. Blicharska,[5] J. Brzychczyk,[6] A. Bonasera,[2] B. Borderie,[7] R. Bougault,[8] G. Cardella,[1] S. Cavallaro,[2] M. B. Chatterjee,[10] A. Chbihi,[11] M. Colonna,[2] R. Dayras,[12] E. De Filippo,[1] M. Di Toro,[2] J. Frankland,[11] E. Galichet,[2,7] W. Gawlikowicz,[18] E. Geraci,[9] G. Giuliani,[1] F. Giustolisi,[2] A. Grzeszczuk,[5] P. Guazzoni,[13] D. Guinet,[14] M. Iacono-Manno,[2] S. Kowalski,[5] E. La Guidara,[2] G. Lanzalone,[2] G. Lanzanò,[1] C. Maiolino,[2] Z. Majka,[6] N. Le Neindre,[7] A. Pagano,[1] M. Petrovici,[4] E. Piasecki,[15] S. Pirrone,[1] R. Płaneta,[6] G. Politi,[1] A. Pop,[4] F. Porto,[1] F. Rizzo,[2] E. Rosato,[16] S. Russo,[13] P. Russotto,[2] M. Sassi,[13] K. Schmidt,[5] K. Siwek-Wilczyńska,[15] I. Skwira,[15] A. Sochocka,[6] L. Świderski,[15] A. Trifirò,[3] M. Trimarchi,[3] G. Vannini,[9] G. Verde,[1] M. Vigilante,[16] J. P. Wieleczko,[11] J. Wilczyński,[17] L. Zetta,[13] and W. Zipper[5]

[1]*INFN, Sezione di Catania and Dipartimento di Fisica, Università di Catania, Italy*
[2]*INFN, Laboratori Nazionali del Sud and Dipartimento di Fisica, Università di Catania, Italy*
[3]*INFN, Gruppo Collegato di Messina and Dipartimento di Fisica, Università di Messina, Italy*
[4]*Institute for Physics and Nuclear Engineering, Bucharest, Romania*
[5]*Institute of Physics, University of Silesia, Katowice, Poland*
[6]*M. Smoluchowski Institute of Physics, Jagellonian University, Cracow, Poland*
[7]*Institut de Phisique Nucléaire, IN2P3-CNRS, Orsay, France*
[8]*LPC, ENSI Caen and Universitè de Caen, France*
[9]*INFN Sezione di Bologna and Dipartimento di Fisica, Università di Bologna, Italy*
[10]*Saha Institute of Nuclear Physics, Kolkata, India*
[11]*GANIL, CEA, IN2P3-CNRS, Caen, France*
[12]*DAPNIA/SPhN, CEA-Saclay, France*
[13]*INFN, Sezione di Milano and Dipartimento di Fisica, Università di Milano, Italy*
[14]*IPN, IN2P3-CNRS and Université Claude Bernard, Lyon, France*
[15]*Institute for Experimental Physics, Warsaw University, Warsaw, Poland*
[16]*INFN, Sezione di Napoli and Dipartimento di Fisica, Università di Napoli, Italy*
[17]*A. Sołtan Institute for Nuclear Studies, Swierk-Warsaw, Poland*
[18]*Heavy Ion Laboratory, Warsaw University, Warsaw, Poland*

(Received 9 February 2007; published 23 May 2007)

Multi-breakup processes for the ^{124}Sn+^{64}Ni system at 35 MeV/nucleon have been studied with the forward part of the CHIMERA detector. An extensive comparison between experimental data corresponding to almost complete ternary events and constrained molecular dynamics (CoMD-II) calculations suggests different characteristic times in the selected processes. This is in agreement with previous studies of the same reaction already published concerning the prompt intermediate-mass-fragment emission. Stimulated by CoMD-II calculations, we investigate the existence of more complex dynamical multi-breakup processes occurring on the same time scale. A detailed study of the rotational dynamics leading to slower dynamical fission processes is also presented.

DOI: 10.1103/PhysRevC.75.054616 PACS number(s): 25.70.Mn, 24.10.Cn, 25.70.Pq

I. INTRODUCTION

One of the most challenging subjects in the study of nuclear reactions at Fermi energies [1] is understanding the basic mechanisms leading to fragment formation [2–8]. In particular, these mechanisms are determined by the fast time evolution of the initial nuclear ground-state structure, which undergoes a great modification of the local densities. Therefore, by studying fragment production, according to different time characteristics, from prompt emission to a more delayed and sequential emission, we could explore the different stages of dynamical evolution, which is sensitive to different kinds of effective interactions modeled by the local densities [9,10]. Another aspect involves the nature of the process itself. It is well known that a wide class of experimental data regarding multifragmentation processes can be reasonably well described by statistical models [11,12] in which the time variable disappears (at least as an independent variable of the problem) whereas others variables, more familiar to the macroscopic world, such as temperature and volume, play the most important role. These cases are normally considered examples of complicated processes that are probably long enough to reach partial equilibrium of the hot sources. In this multifaceted context, the experimental identification of complex processes with clear dynamical features acquires a remarkable relevance. In this article, particular emphasis has been given to the dynamical aspects frequently using the term multi-breakup rather than multifragmentation, to indicate processes that produce more than two fragments.

The system ^{124}Sn+^{64}Ni at 35 MeV/nucleon was investigated by means of the forward part ($1^\circ < \theta_{lab} < 30^\circ$) of the Charge Heavy Ion Mass and Energy Resolving Array (CHIMERA) [13] in the reverse configuration. The advantage

of focusing the reaction products at the forward angle dictated the choice of a reaction in the inverse kinematics. The target-like fragment (TLF) has to be fast enough in the laboratory system in order to be detected while the velocities of the projectile-like fragment (PLF), the intermediate-mass fragment (IMF), and the TLF have to be sufficiently differentiated. For these reasons, the ^{124}Sn+^{64}Ni system at projectile energy $E(^{124}\mathrm{Sn}) = 35$ MeV/nucleon was chosen for the present experiment.

Clear dynamical effects have been shown in Refs. [14,15], for the almost complete ternary events generated in mid-peripheral collisions. The possibility of detecting both the PLF and TLF allowed us to study relative velocity correlations with the IMF partner. In such studies, a chronological order regarding the emission of the IMFs was observed, from short periods of time related to the formation of "mid-rapidity" IMFs (the so-called neck emission) to longer ones characteristic of a sequential PLF and TLF fragment decay.

The aim of this work is to perform a global analysis to illustrate the different dynamical aspects of the multi-breakup processes observed. In particular, in Sec. II we review results related to the so-called ternary events [14]. In Sec. III, we discuss the evidence of more complex multiple breakup contributions occurring on the same time scale related to the TLF primary sources. In Sec. IV we analyze the dynamical fission events [15] and we include an investigation of the rotational dynamics of the pre-fission PLFs. Finally, in the Appendix the connection between the average fission time and the average angular velocity of the pre-fission nucleus is discussed in some detail.

The analysis and dynamical nature of all these breakup processes will be discussed within the framework of the Constrained Molecular Dynamical-II (CoMD-II) model [16, 17]. This self-consistent N-body approach overcomes the main problems typically related to semiclassical many-body dynamics [18–23] by solving the equations of motion using constraining procedures to fulfill the Pauli principle (event after event) and to respect the conservation rule regarding the total angular momentum. This last feature plays a crucial role in producing dynamical processes with different time characteristics and it has also been used to describe fragment-Giant Dipole Resonance (GDR)-γ-ray coincidence measurements [17].

In particular, we generated several tens of thousands of events with the CoMD-II model up to a maximum time of 800 fm/c and for impact parameters b ranging from 0 fm to $0.85b_{\max}$($b_{\max} \approx 10.5$ fm). The calculations have been filtered by using the response function of the CHIMERA apparatus, taking into account the thresholds of kinetic energy and trigger multiplicity. Even if the angular coverage of the reverse configuration has not been considered for problems related to the simulation statistics, the main kinematical restrictions, coming from the selection of fragment velocities applied to the data analysis, have been properly taken into account when being compared to experimental data. Also, owing to the relatively long time (800 fm/c) in which the dynamical evolution had been studied, a part of the secondary evaporation process of the hot fragments is consequently taken into account. These limitations, therefore, make the level of our comparison semiquantitative. However, it will be shown in the following sections that the main correlations related to the time of the processes and the size and velocity of the fragments have been reproduced in a satisfactory way. This in turn gives an empirical basis to the interpretation (also at a microscopic level) of the dynamics related to the studied process as obtained from our calculations.

II. TERNARY EVENTS

A. Main selection criteria

We studied the system ^{124}Sn+^{64}Ni at 35 MeV/nucleon with the forward part of the CHIMERA detector and, in this section, we discuss the experimental results obtained by selecting events with at least three fragments with charge $Z \geqslant 3$ and that fulfill the following conditions: $P^d_{\mathrm{tot}} \geqslant 0.65 P_{\mathrm{tot}}$ and $Z^d_{\mathrm{tot}} \geqslant 55$. Here P_{tot} is the linear momentum of the total system and Z^d_{tot} and P^d_{tot} represent the the total charge and the total linear momentum of the detected fragments, respectively. For these events in Fig. 1(a) we show the correlation between the charges of the three biggest fragments and their velocities along the beam direction, V_{par}. From the figure it can be seen that the aforementioned conditions mainly select events that include the PLF, the TLF, and one IMF with a parallel velocity in the mid-rapidity region. Therefore, even if these selection criteria are slightly less restrictive than the one used in Ref. [14], we will name these events ternary in accordance with the same work. These conditions give a first selection level that is also applied to the analysis discussed in the next sections. Details on the CHIMERA detector and on its ability to measure the charge, mass, and velocity of particles according to their size, energy, and direction are reported in Ref. [13].

B. Charge-velocity correlations and time scales

Figures 1(b) and 1(c) show the results of CoMD-II calculations corresponding to the indicated impact parameter b ranges in units of $b_{\max}$.

In particular, the charges and velocities of the three biggest fragments with $Z \geqslant 3$ are shown in Fig. 1(b). These quantities display correlations that are very similar to the experimental ones [Fig. 1(a)]. The dynamical calculations also indicate that the shape of such a correlation plot sensitively depends, as expected, on the selected b window. In Fig. 1(c) CoMD-II results for smaller impact parameters are shown. In this case one has, on average, the survival of a PLF fragment with a lower velocity, whereas the charge of the TLF residue is considerably reduced and the velocity is increased. Therefore, we notice the tendency of the TLF residue fragments to populate a region that is usually filled by the IMF of intermediate velocity produced by more peripheral reactions. From the plots in Fig. 1, it is clearly seen that in this case the so-called 'neck formation process can merge with the TLF multi-breakup [24].

Other interesting velocity correlations reported in Ref. [14] are more closely related to the time scale of these processes. In Fig. 2(a) we show the plot of the experimental reduced relative velocity of the IMF (third biggest fragment) with respect to the TLF fragment, $V^{\mathrm{IT}}_{\mathrm{red}}$, as function of its reduced velocity

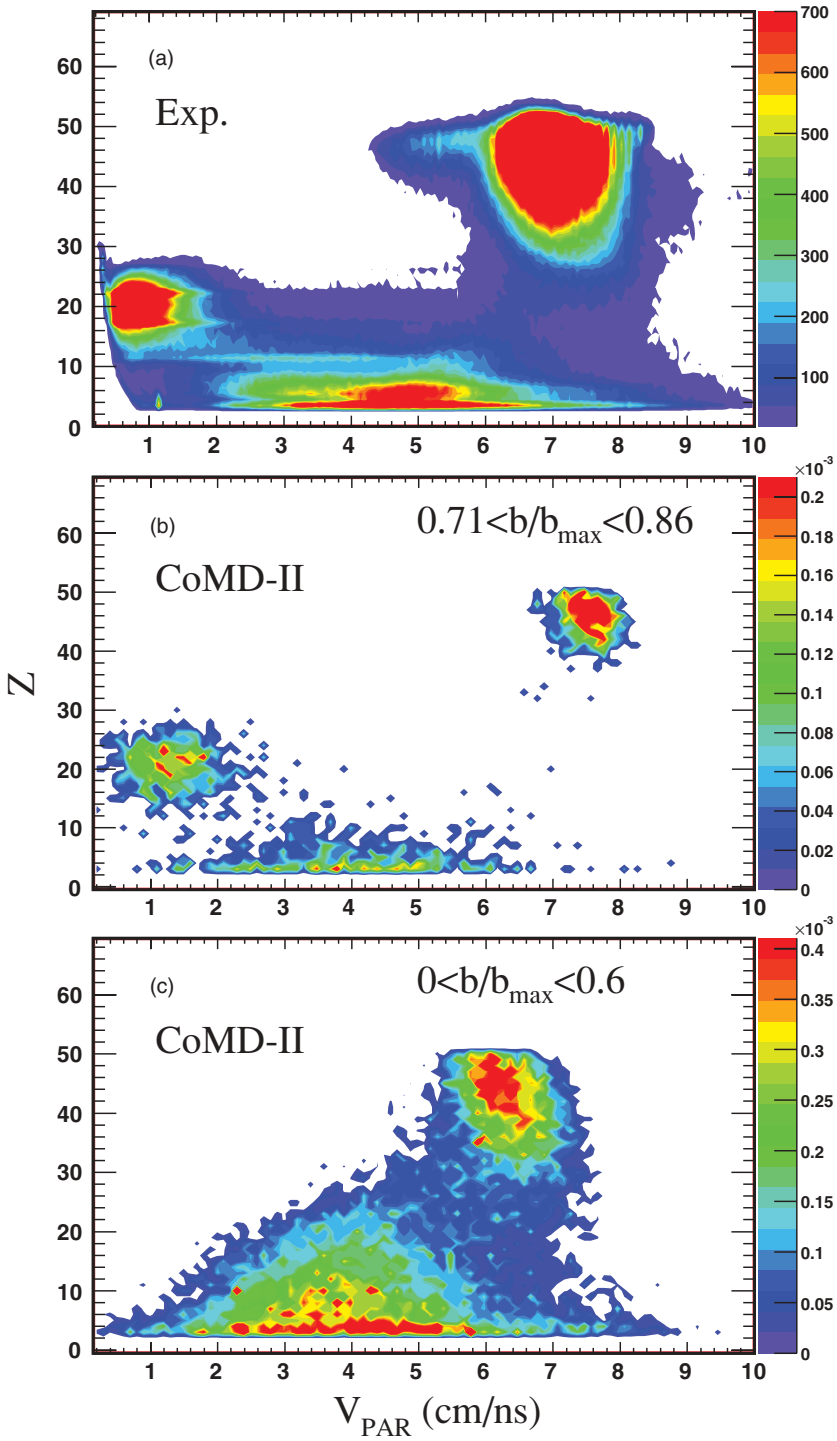

FIG. 1. (Color online) (a) Experimental charge Z vs parallel velocity $V_{\rm par}$ plot for the three biggest fragments with $Z \geqslant 3$. The color scale on the right-hand side of the panel shows the number of counts per two-dimensional bin. (b), (c) The analogous plots evaluated with the CoMD-II model for different windows of impact parameter b. The color scale is in arbitrary units.

with respect to the PLF, $V_{\rm red}^{\rm IP}$. As usual, the quantities $V_{\rm red}^{\rm IT}$ and $V_{\rm red}^{\rm IP}$ represent the relative velocities of the IMF divided by the corresponding value obtained from the Viola systematics [25].

In Ref. [14] the average correlation shown in the figure has been calibrated in time by using a basic three-body kinematics model. This includes the mutual Coulomb interactions between fragments and the use of simple assumptions about their relative distances and velocities. In particular, it was shown that processes with the shortest emission time, corresponding to IMF velocities around the mid-rapidity region, fill, on average, the central region of the $V_{\rm red}^{\rm IT}$-$V_{\rm red}^{\rm IP}$ plot along characteristic lines that depend on the model parameters (see Ref. [14] for more details). This is seen more clearly by comparing Fig. 2(a) with Fig. 2(b), which represents the experimental results obtained for IMF velocities ranging between 2.5 and 5 cm/ns. More delayed sequential processes should fill the region along the axes. These last cases correspond to prompt binary processes followed by a delayed PLF or TLF fission.

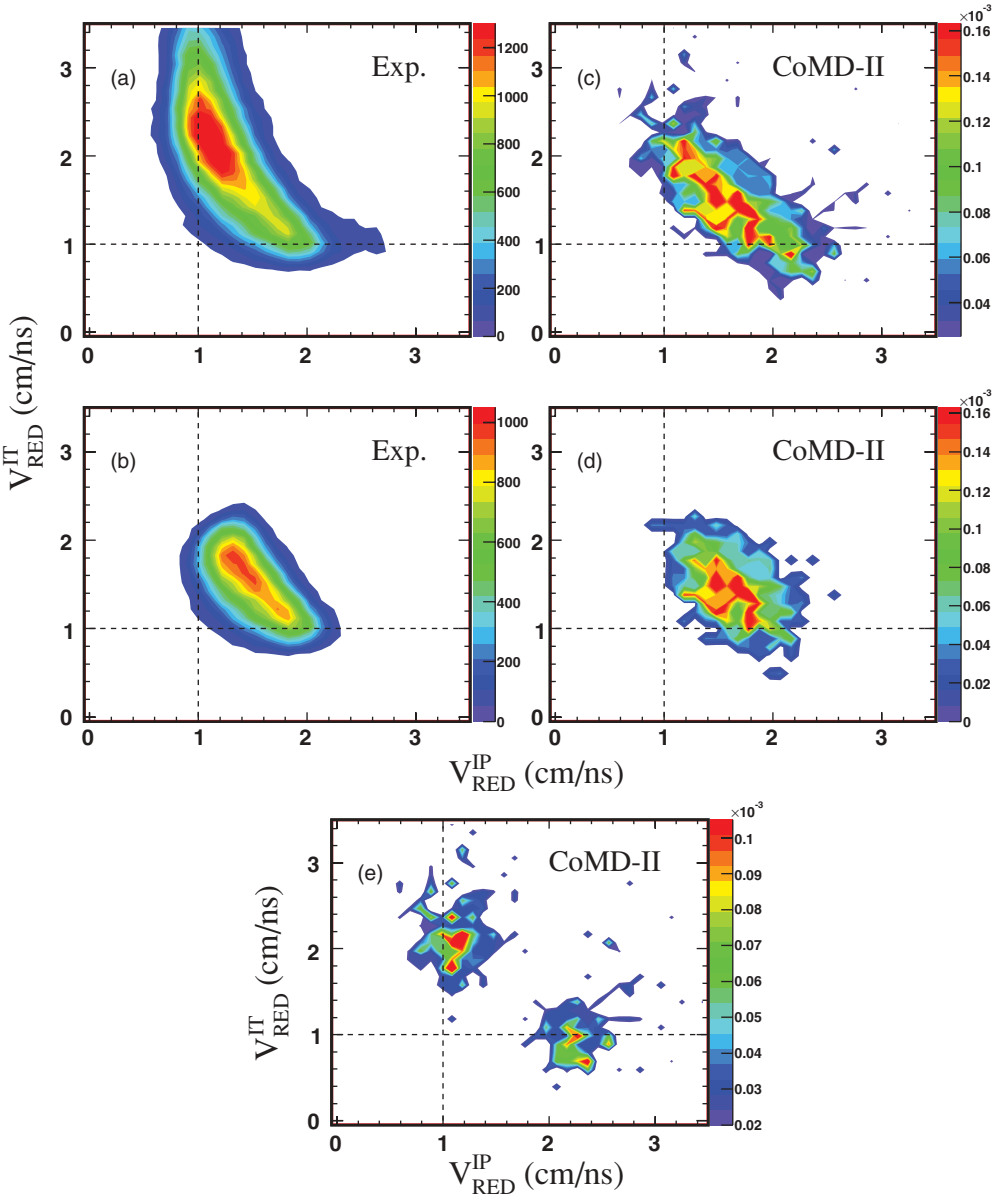

FIG. 2. (Color online) In panels (a) and (b) we show the experimental V^{IT}_{red}-V^{IP}_{red} plots for ternary events. In panel (b) only IMFs having a velocity range of 2.5–5 cm/ns have been considered. The color scale on the right-hand side of the panel shows the number of counts per two-dimensional bin. Panels (c) and (d) show the analogous plots obtained from CoMD-II calculations. Panel (e) shows the calculation results obtained for IMFs velocities outside the range 2.5–5 cm/ns. The color scale is in arbitrary units.

The study performed in Ref. [14] allowed us to evaluate a separation time for mid-rapidity IMFs ranging between 40 and 120 fm/c. The corresponding plots obtained from CoMD-II calculations are shown in Fig. 2(c) and Fig. 2(d), respectively. From Fig. 2(d) we can see that the experimental correlations close to the mid-rapidity IMF velocities are well reproduced. However, the greater yield seen in Fig. 2(a) along the $V^{IP}_{red} = 1$ axis, corresponding to a longer time scale toward the PLF fission, is not reproduced in Fig. 2(c). This could be connected to the finite time of the calculations.

Nevertheless, in Fig. 2(c), the region along the $V^{IP}_{red} = 1$ axis is not empty. This is clearly seen in Fig. 2(e), where we show the calculated V^{IT}_{red}-V^{IP}_{red} plot for IMF velocities outside of the range 2.5–5 cm/ns. The simulated events that fill the region along the $V^{IP}_{red} = 1$ axis include the PLF fission evolving with an average decay time of about 300 fm/c and producing an IMF with an average mass of about 35 units. This is clearly seen in Fig. 3, where the open circles show the time evolution of the average masses calculated for the three biggest fragments A_1, A_2, and A_3 for the process selected. We see that this evolution is characterized by a "time delay" (the time that the total system spends in a compact configuration with $A_1 \approx 188$) of about 130 fm/c. The TLF (A_2) is formed after about 50 fm/c and the PLF (A_1) undergoes a binary splitting in the subsequent time interval of about 300 fm/c. In the same part of the figure, the full dots refer to the same quantities

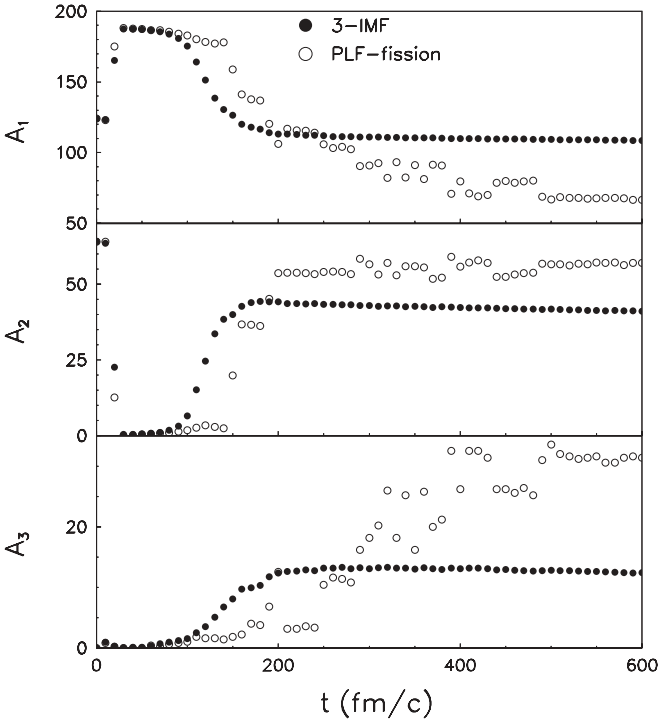

FIG. 3. Time evolution of the average mass numbers of the three biggest fragments according to the CoMD-II model for ternary (full dots) and dynamical fission events (open circles).

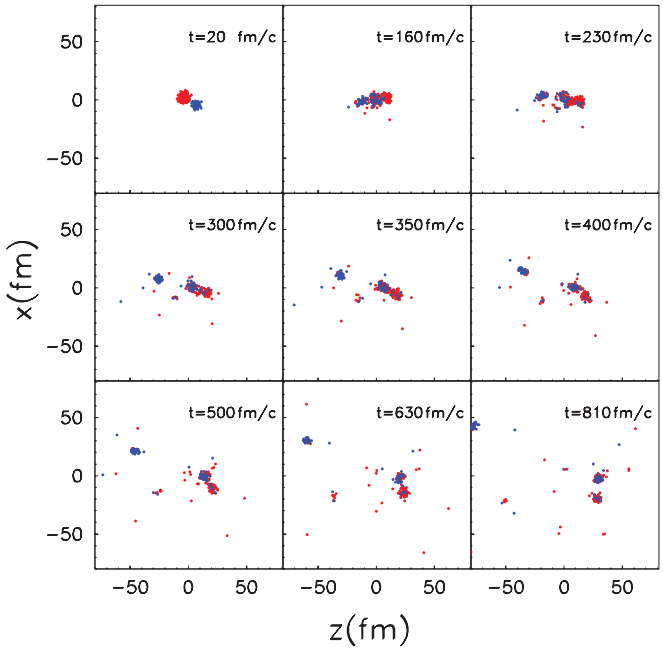

FIG. 4. (Color online) Configurational map, at different time steps, of one event related to the ^{124}Sn+^{64}Ni system at 35 MeV/nucleon leading to the fission of the heavy partner.

related to ternary events corresponding to the selected events of Fig. 2(d). In this case, for the three fragments, we obtain a time delay and a formation time of about 70 fm/c; therefore the character of the breakup process can be described through a faster simultaneous mechanism. This last prompt mechanism was also reproduced in the framework of stochastic BNV (Boltzman-Nordheim-Vlasov) calculations [26].

Finally, in Fig. 4 we show configurational maps calculated at different times representing a typical event evolving with the longer time scale and leading to a PLF fission event. We conclude this section by observing that to reproduce these different characteristic times with the CoMD-II approach, it has been necessary to constrain the equations of motion to fulfill the total angular momentum conservation law [17]. This conservation principle is violated in all the microscopic approaches that use random impulsive forces (as for example the ones necessary to simulate the nucleon-nucleon hard-core interaction) without including dedicated algorithms to overcome the problem [27].

III. MORE COMPLEX MULTI-BREAKUP PROCESSES

In this section, we show the results of an analysis devoted to revealing a class of events that can be interpreted as corresponding to a light partner multi-breakup. To do this, we have divided the fragment velocity space into two regions: the so-called TLF side, corresponding to fragments having negative parallel velocity values [calculated in the center-of-mass reference (c.m.) system], and the complementary region, which corresponds to the PLF side. Among the well-reconstructed experimental events, according to the criteria mentioned in the previous section, we have selected those fulfilling the following conditions. We have considered all the events having a multiplicity of charged fragments, detected on the TLF side, greater than three. The total charge $Z_{\rm ntg}$ of the detected particles on the TLF side changes within the interval $20 < Z_{\rm ntg} < 34$. Moreover, we have applied further restrictions regarding the size of the three biggest fragments with charges Z_{d1}, Z_{d2}, and Z_{d3} (produced on the TLF side). Their total charge Z_d is less than $0.8Z_{\rm ntg}$ and the distance D_d of the related Dalitz variables $C_1 = \frac{Z_{d1}}{Z_d}$, $C_2 = \frac{Z_{d1}+2Z_{d2}}{Z_d\sqrt{3}}$ from the center of the characteristic triangle ($C_1^0 = \frac{1}{3}$, $C_2^0 = \frac{1}{\sqrt{3}}$) is less than 0.26. These restrictive conditions aim to select complex processes in which the TLF breaks into light particles and at least three IMFs with a limited mass asymmetry. Therefore, it is difficult to interpret this process as produced through sequential statistical TLF decay. For these events in Fig. 5 we have shown, as a function of time, the average mass A_1 of the biggest fragment (PLF fragment) and the average masses of the three biggest fragments, A_{d1}, A_{d2}, and A_{d3}, produced on the TLF side. From the figure, we can note that the multi-breakup process is simultaneous and evolves almost within the same time scale of ternary events (see Fig. 3). For the same events, in Fig. 6 we show a comparison between the model calculations and the experimental data concerning the Dalitz and the Z-$V_{\rm par}$ plots for particles with $Z \geqslant 3$. The overall comparison, involving the correlations in charge, velocity, and size of at least four fragments is satisfactory.

Most relevant differences are concerned with the charge of the PLF. In about 75% of cases, the charge of the biggest fragment detected on the PLF side is less than 30 units. The calculations, instead, produce a higher average value. The

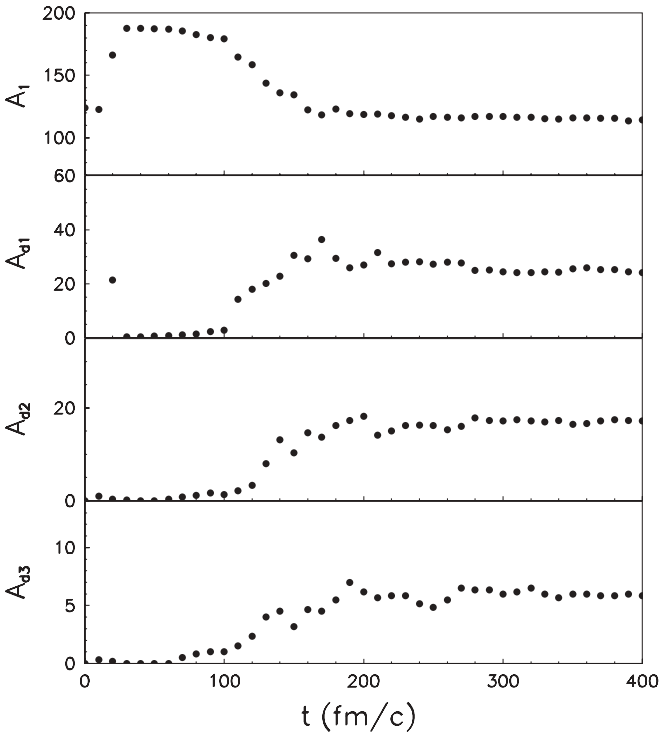

FIG. 5. Time evolution for the average masses of the four biggest fragments produced in more complex multi-breakup processes evaluated through CoMD-II calculations.

coupling of CoMD-II calculations with a statistical model that describes the secondary stage of cooling of the biggest fragments can improve the agreement.

In the following part of this section, we present a comparison concerning the degree of centrality and the energy balance between the described complex multi-breakup processes and the so-called ternary events producing at least one IMF (1-IMF process) and a PLF with a parallel velocity grater than 6.5 cm/ns. In Fig. 7(a) the dashed and continuous lines show the impact parameter distributions for 1-IMF and 3-IMF multi-breakup processes, respectively. These have been obtained from CoMD-II calculations. The dotted line represents the impact parameter distribution used in the simulations (which is linear in b). From the figure we can see that 3-IMF processes are a small fraction (about 10%) of the more frequent 1-IMF events and that the corresponding b window is shifted to smaller impact parameters.

To compare the related degree of energy dissipation, as obtained from CoMD-II calculations, we have reduced the configuration of the final system into a binary one. The charges, masses, excitation energies, binding energies, and relative kinetic energies of all fragments and particles produced on the TLF side have been composed to define a virtual source (not really observed) with a proper c.m. velocity. It has been labeled with the number 2 in Fig. 7(c). The same procedure has been applied to fragments and particles produced on the PLF side giving rise to a virtual source, which we have labeled with the number 1 in the same figure. In Fig. 7(b) we can see the total kinetic energy loss (T_{KEL}) spectrum for 3-IMF events (continuous line) and for 1-IMF ones (dashed line) obtained through the reconstructed c.m. velocities. From the figure it is evident that the 3-IMF events give rise to more dissipative processes (with an average T_{KEL} value of about 750 MeV) with respect to the 1-IMF events (with an average T_{KEL} value of about 536 MeV). In TLF multi-breakup processes, the average experimental value of T_{KEL} deduced from the two virtual sources can be roughly estimated by considering, on average, 20% of undetected mass. A value of about 785 MeV is obtained, which is in satisfactory agreement with the calculations. The different degree of dissipation also affects the excitation energies of the two virtual sources, E_1^* and E_2^*, as shown in Fig. 7(c). In particular, E_2^* for the 3-IMF processes is, on average, equal to 6.5 MeV/nucleon, about 1.5 MeV/nucleon higher than the one related to the ternary events. Finally, we can see that the reconstruction of these two virtual sources allows us to show that the two mechanisms involved produce a relevant difference between the excitation energy per nucleon absorbed on the TLF and PLF sides. This further confirms the high nonequilibrium character of the processes investigated.

Now, we would like to briefly describe the mechanism of the TLF multi-breakup at a microscopic level. The left part of Fig. 8 refers to projectile nucleons, and it shows the average density evaluated at different times on the entrance reaction plane. In the right panels of Fig. 8 similar plots are shown for target nucleons. The reference system corresponds to the c.m. reference frame.

From the figure it appears that a substantial fraction of the target mass is transferred into the region where most of nucleons form the projectile nucleus (half-space with $z > 0$). Within the same time scale, other nucleons are transferred from the projectile to the target side (half-space with $z < 0$). There, net transfer of mass is small and the remaining nucleons of the target form a region of low density in which the nucleons coming from the projectile are involved in the cluster formation. In contrast, the nucleons of the target migrating into the projectile side are on average bound by the stronger projectile mean field. In fact we can see in Fig. 8 that, for $z > 0$, the target nucleons form an almost compact region in density distribution, embedded in the corresponding more dense and extended region of projectile nucleons, to form the PLF nucleus. As a result, the TLF undergoes the multi-breakup process. Therefore, the process seems to be triggered by the fast stripping of a non-negligible fraction of the target mass in the projectile mean field. This stripping generates the instability of the lighter partner, which now includes a similar fraction of projectile nucleons.

IV. PLF ROTATIONAL AND FISSION DYNAMICS

To complete the study of the main multi-breakup processes in the system under investigation we should discuss some aspects related to so-called dynamical fission, already observed around 20 MeV/nucleon [28] and at higher energy [6,15,29]. This process, induced by the violent collision between the target and the projectile, produce the fission of one of the two partners (in this work the projectile) into two nuclei having a limited mass asymmetry. It is characterized by a remarkable

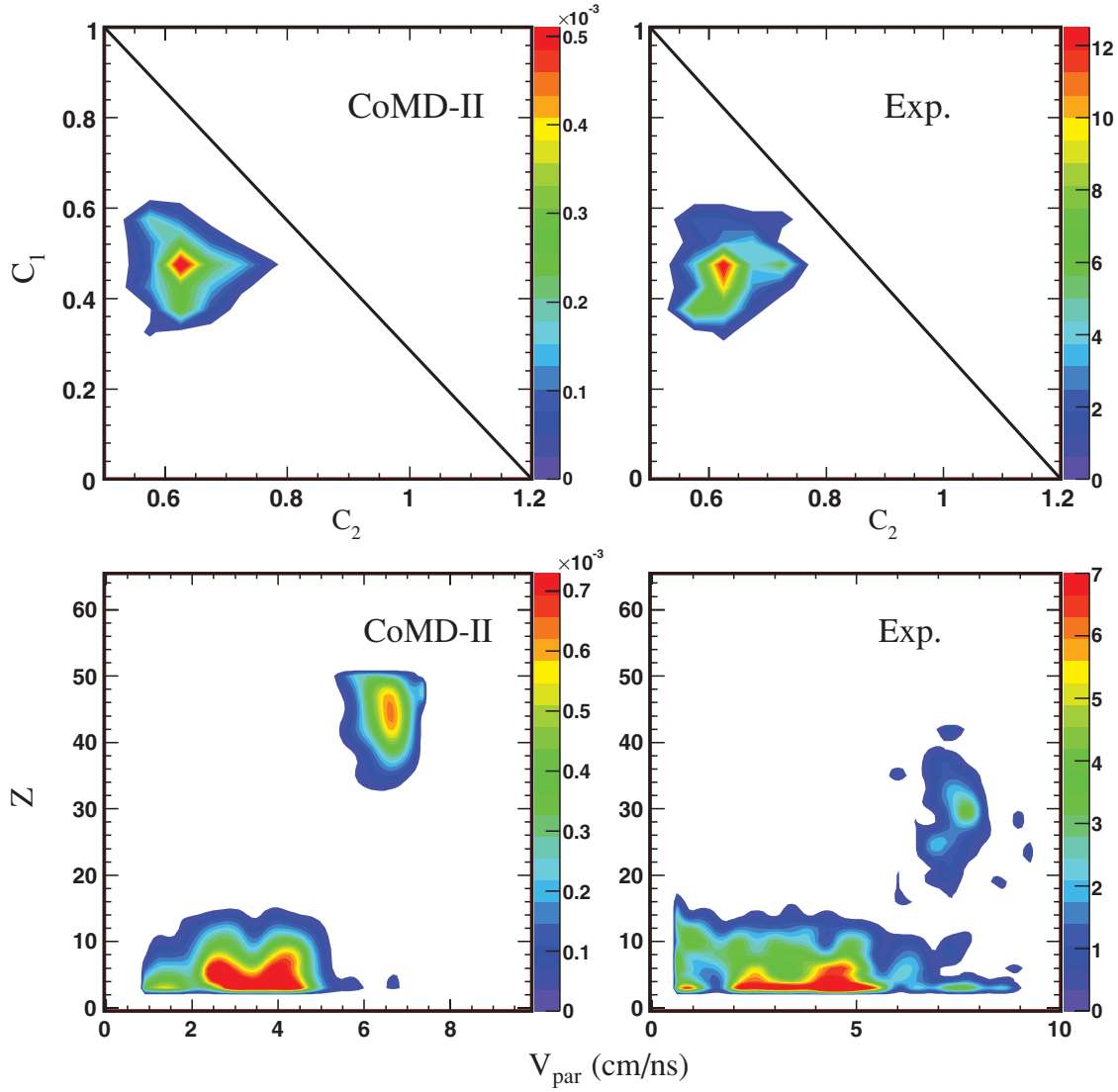

FIG. 6. (Color online) In the upper part calculated and experimental Dalitz plots are shown for the three biggest fragments of the so-called TLF multi-breakup. In the bottom part the related Z-V_{par} correlation plots are also shown. For the experimental data the color scale on the right-hand side of the panel shows the number of counts per two-dimensional bin. For CoMD-II calculations the color scale is in arbitrary units.

alignment of the three main fragments, producing a focusing of the Φ_{plane} distribution at small angles (see the following text). This means that the relative motion of the fission products "remembers" the direction of the generating violent collision between target and projectile. By contrast statistical fission will produce a flat contribution of the Φ_{plane} distribution.

According to the results obtained in Ref. [15] and the study performed in Sec. II (see Figs. 3 and 4), in ternary events a large contribution from a sequential breaking of the hot compound is visible for moderate asymmetry between the masses of the PLF and the IMF produced at mid-rapidity. These events also show a Φ_{plane} distribution strongly peaked at forward angles. The angle Φ_{plane} is defined [28] as the oriented angle between the projection of the fission axis and of the separation axis on the reaction plane. Figure 9 shows a schematic picture indicating the definitions of these axes and the related in- and out-plane angles [15]. The average value of Φ_{plane} ($\overline{\Phi_{plane}}$) is an observable having an important meaning. In fact it contains implicitly the information related to the characteristic time of the process. To extract this information, one needs to know both the rotational and fission dynamics. At this energy, however, the characteristic time intervals of the processes leading to dissipation, transfer of angular momentum, and the formation and splitting of the hot fragments can be partially overlapped (see the following text). Therefore, in this case, simple models based on rigid-body rotation, the transfer of spin, and the subsequent fission could be inadequate. In this context, the possibility of producing hot sources able to rotate in a collective way should also be examined. In particular, for the system under study, these problems were raised in Ref. [15] to better understand the relatively small value of the observed $\overline{\Phi_{plane}}$.

In this section we present the results of CoMD-II calculations aimed at revealing the interplay between the rotational

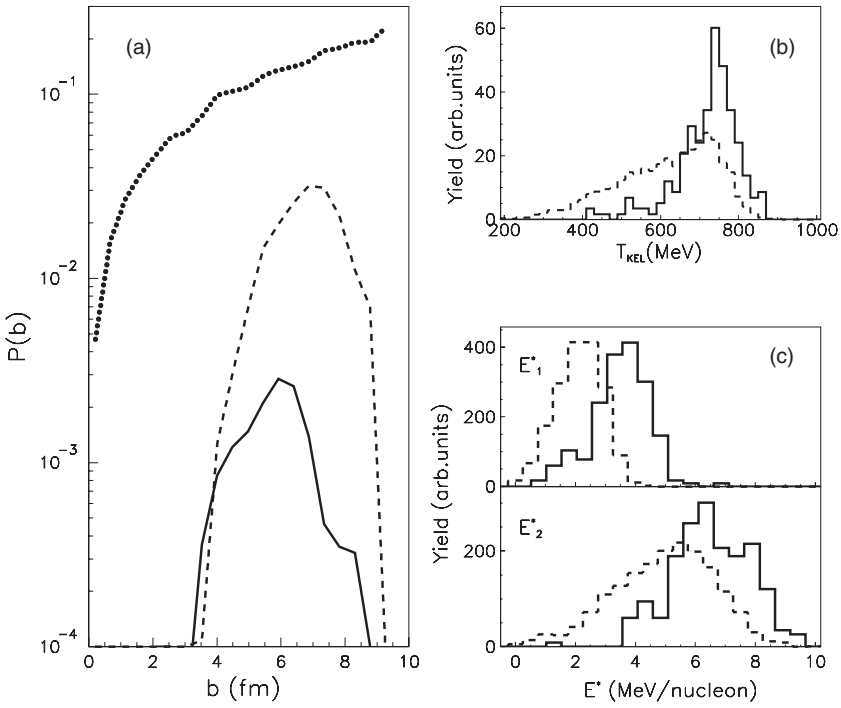

FIG. 7. (a) Impact parameter distributions from the CoMD-II calculation. The dotted line represents the distribution used in the simulations. The dashed line is the distribution obtained for the selected ternary events (one IMF process); the continuous line is related to events with at least three IMFs produced in the target side (see text). (b) Calculated T_{KEL} spectra related to ternary events (dashed lines) and TLFs multi-breakup events (continuous lines). (c) Evaluated intrinsic excitation energies E^*_1, E^*_2 related to the two virtual sources reconstructed from CoMD-II calculations in the PLF and TLF sides, respectively. The dashed line refers to ternary events whereas the continuous one is related to TLF multi-breakup events.

and fission dynamics and trying to give a self-consistent interpretation of the measured $\overline{\Phi_{\mathrm{plane}}}$. We also note that, for moderate asymmetric splitting, CoMD-II calculations predict longer average formation times with respect to more asymmetric IMF emissions (neck emission; see Fig. 3).

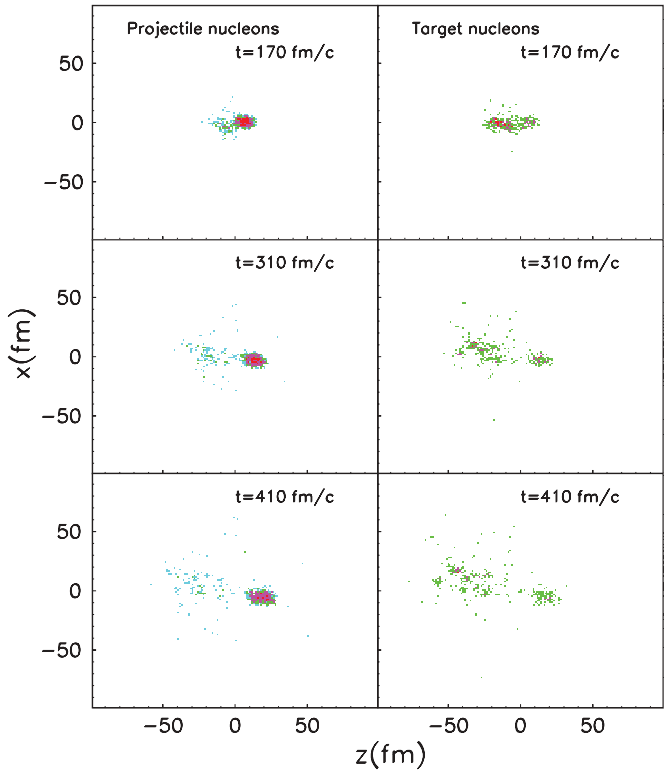

FIG. 8. (Color online) Average density plots on the entrance reaction plane, evaluated at different times, related to projectile (left column) and target nucleons (right column) for TLF multi-breakup processes. In particular, because of the kinematics of process the PLF and TLF regions are located in the $z > 0$ and $z < 0$ half-spaces, respectively.

Figure 10 shows a comparison between the experimental Φ_{plane} distribution and the calculations obtained from an analysis of ternary events. In particular, the open circles indicate the experimental results obtained by selecting IMFs emitted with a velocity greater than $V_{\mathrm{thr}} = 3$ cm/ns and with a ratio between the masses of the PLFs and IMFs (A_{HL}) less than five. In the same figure, CoMD-II results are plotted with full dots. They have been obtained for the same values of V_{thr} and A_{HL}.

Model calculations reproduce the experimental Φ_{plane} distribution well, including the value of $\overline{\Phi_{\mathrm{plane}}}$ (about 10 degrees) and the background associated with the primary PLF splitting processes with longer emission times. This almost flat contribution is also understandable in the framework of conventional statistical emission.

To investigate rotational dynamics in more detail, we calculated spins and related angular velocities for different parts of the system, starting from a full microscopic description of the system in terms of nucleon positions, velocities, and momenta, $\vec{r_i}$, $\vec{v_i}$, and $\vec{p_i}$, respectively. The coordinates of the generic nucleon i refer to the c.m. system of the fragment to which the nucleon belongs. For a generic fragment with mass number A^f_k produced in the kth event and belonging to the class f (the total system, the biggest one, the second biggest one, and so on), the ensemble average has been evaluated on the N selected events ($A_{\mathrm{HL}} < 5$) in times step of 5 fm/c, according to the following equations:

$$\Omega^f = \frac{1}{N}\sum_k \omega^f_k; \quad \omega^f_k = \frac{1}{A^f_k}\left(\sum_i \frac{\vec{r}^{\,f}_{i,k} \times \vec{v}^{\,f}_{i,k}}{\left(x^{2f}_{i,k} + z^{2f}_{i,k}\right)}\right)_y, \qquad (1)$$

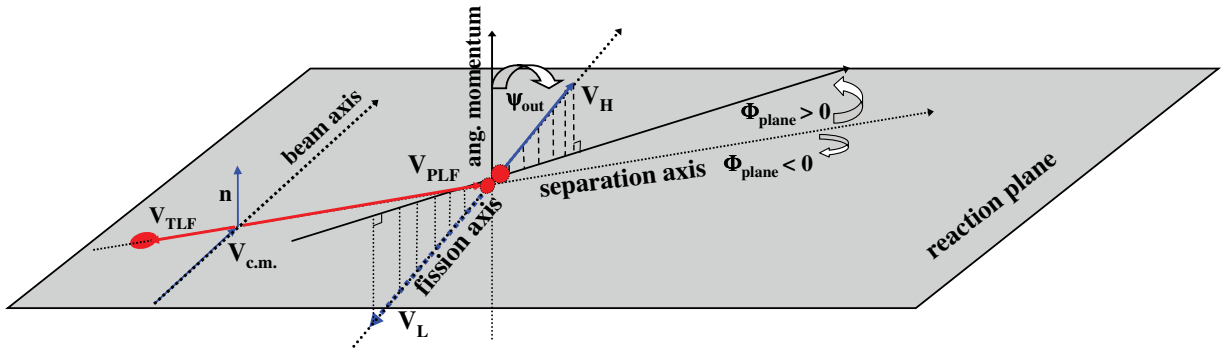

FIG. 9. (Color online) Schematic picture showing the definition of the in-plane Φ_{plane} and out-plane Ψ_{plane} angles.

$$\Omega_c^f = \frac{1}{N}\sum_k \omega_{c,k}^f; \quad \omega_{c,k}^f = \frac{J_k^f}{I_k^f}, \tag{2}$$

$$J_k^f = \left(\sum_i \vec{r}_{i,k}^{\,f} \times \vec{p}_{i,k}^{\,f}\right)_y, \tag{3}$$

$$I_k^f = m_0 \sum_i x_{i,k}^{2f} + z_{i,k}^{2f}, \tag{4}$$

$$J^f = \frac{1}{N}\sum_k J_k^f, \tag{5}$$

where m_0 is the nucleon mass. In the previous expressions, according to the CoMD-II results on the ensemble averages, the off-diagonal terms related to the inertia parameters have been omitted since they are small. Negligible values were also obtained for the average angular velocities and spins along the $\hat{x}$ and $\hat{z}$ directions, which define the entrance reaction plane. However, huge fluctuations are present and they are responsible for out-plane distributions, which we do not discuss in the present work. It is worth noting that, according to Eqs. (1) and (2), a substantial rotational collectivity for the generic fragment motion is obtained if $\Omega_c^f \approx \Omega^f$. The angular velocity Ω^f is in fact defined through the quantities ω_k^f, which represent, for each fragment, the microscopic average angular velocity, whereas Ω_c^f is defined through the $\omega_{c,k}^f$ quantities, which represent the collective values of the angular velocity obtained through the typical relationship characterizing the rigid-body motion. In Fig. 11(a) we show the average value of the spin for different parts of the system during the fragment formation process as a function of time. The small closed dots represent the total angular momentum J^{tot} for the selected processes, which is well conserved according to the CoMD-II features. The other symbols represent the spin for the main fragments along the direction $\hat{y}$ normal to the reaction plane. The term $J^{1,3}$ is the total angular momentum related to the system formed by the PLF residue and the third biggest fragment; J^1 indicates the spin of the biggest fragment (which becomes a pre-fission fragment after about 130 fm/c and the PLF fragment at a later time); J^3 is the total angular momentum associated with the third biggest fragment. Finally J^r represents the relative angular momentum for fragments 1 and 3. In Fig. 11(b) the related average angular velocities are also shown.

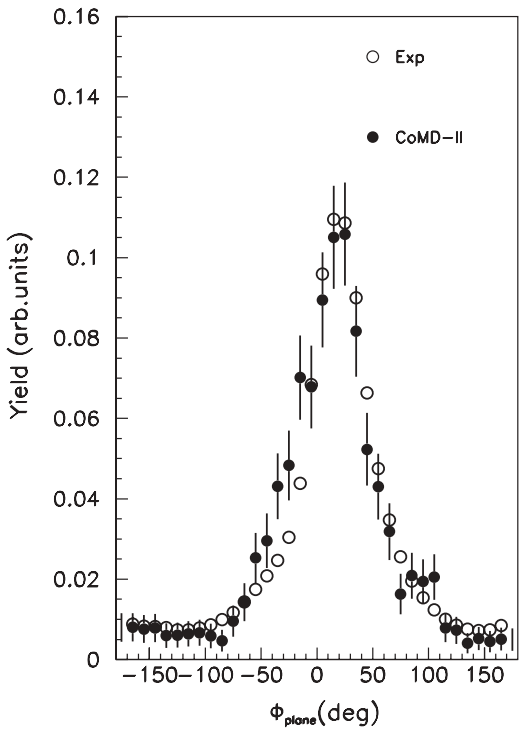

FIG. 10. Experimental and calculated Φ_{plane} distribution for ternary events with $A_{HL} < 5$ and $V_{thr} = 3$ cm/ns. The bars indicate the errors related to the statistics of simulations. For the experimental data the errors are smaller than the size of the symbol.

From Fig. 11(a) we can see that the process leading to the transfer of the angular momentum to the biggest and third-biggest fragments is dominated by strong dissipative effects. The biggest fragment has, on average, a spin value of about 40$\hbar$ at a time of approximately 200 fm/c, whereas the third fragment has a negligible value. The strong dissipation develops in the first 200 fm/c owing to particle emission and the fraction of angular momentum transferred to the TLF during this time interval. Nevertheless, a non-negligible fraction of the total angular momentum is absorbed by the relative motion of the developing binary system formed by the PLF and the mid-rapidity fragment 3. The maximum relative angular momentum J^r is about 120$\hbar$ at 200 fm/c and this value remains

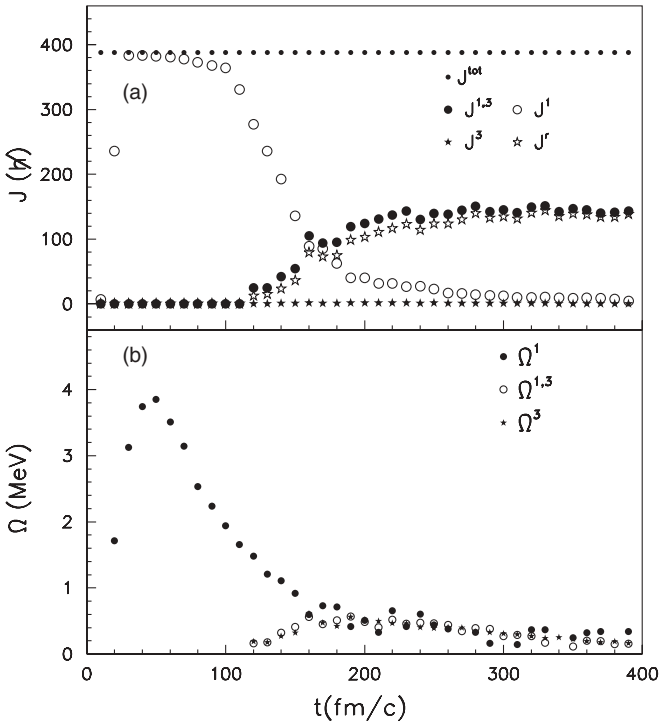

FIG. 11. (a) Calculated intrinsic angular momentum of different parts of the system as a function of time. The small circles represent the total angular momentum. The labels 1 and 3 indicate the biggest and third-biggest fragments. $J^{1,3}$ indicates the total spin of the binary system formed by fragments 1 and 3, whereas J^r is the part associated with relative motion. (b) Related average angular velocities evaluated according to Eq. (1).

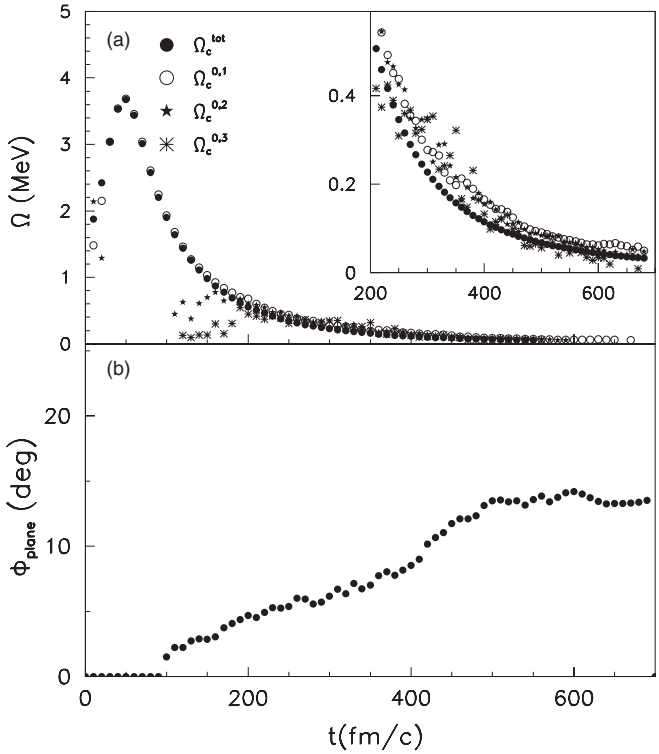

FIG. 12. (a) Average value of the angular velocities calculated for the total system ($\Omega^{\rm tot}$) and its different parts evaluated through Eq. (2). The inset represents an enlargement of the plot in the time interval 200–700 fm/c. (b) $\overline{\Phi_{\rm plane}}$ as a function of time calculated for $A_{\rm HL} < 5$.

almost constant in the subsequent time evolution when the two fragments are definitely separated.

This relative angular momentum and deformation effects are responsible for the dynamical fission of the biggest fragment and produce a low and decreasing value of the relative angular velocity [see empty circles in Fig. 11(b)]. This is due to the rapid increase of the relative moment of inertia, I^r, related to the fragments 1 and 3. In fact, for the class of selected events, on average, the transfer time interval of relative momenta and the splitting time of the biggest fragment partially overlap. Moreover, our calculations indicate that the inertia parameter governing the relative motion between fragments 1 and 3 is about 3,500 fm^2 at 180 fm/c. This high value, which determines the low value of the maximum angular velocity, is due to expansion and hyperdeformation effects experienced at this stage by the fragments involved.

In Ref. [15], according to some indications obtained from BNV calculations, the average alignment angle was related to a complete loss of collectivity for the PLF rotational motion during the first 100–200 fm/c. According to the same results, the collectivity of the PLF rotational motion is restored at a later time when its spin reaches a value of about 30$\hbar$. The CoMD-II results give a different picture: For the biggest fragment between 100 and 150 fm/c, when the PLF fragment is separating from the TLF, the values of Ω_c and Ω are comparable within 5%, reflecting a substantial collective rotation according to Eqs. (1) and (2). Larger deviations, up to a level of about 30%, are predicted at longer time.

For an overall description, we now discuss the degree of collective rotation for the entire system by comparing the angular velocity $\Omega_c^{0,f}$ [obtained by using the formula reported in Eq. (2)] of the main fragments computed with respect to a common pole: the c.m. of the total system. In Fig. 12(a) we have plotted the average angular velocity along the $\hat{y}$ direction. In the figure $\Omega_c^{\rm tot}$, Ω_c^{01}, Ω_c^{02}, and Ω_c^{03} represent the angular velocity of the total system, of the biggest fragment, and of the second- and the third-biggest fragments, respectively. The angular velocity of the total system decreases after about 40 fm/c owing to elongation and expansion effects (non-rigid-body motion). It can be taken as a reference velocity during the time evolution. Almost the same behavior is followed by Ω_c^{01}, still reflecting the substantial collective rotation of the PLFs in the first stage of the collision process. The velocities Ω_c^{02} and Ω_c^{03} increase just during the fragment formation time. During this time interval the Ω_c^{02} and Ω_c^{03} values show the largest deviations from $\Omega_c^{\rm tot}$. This stage is strongly dominated by "sliding" and nucleon transfer effects. After 200 fm/c the main parts of the system have similar angular velocities (within 30%), as can be seen in the inset of Fig. 11(a). Therefore, on the whole, we can say that the entire system does not rotate collectively. In fact, during the time evolution, different parts develop different angular velocity with respect to the same pole. However, the most important noncollective rotational

effects, for the total system, are not related to the biggest fragment or PLF but are associated with the development of TLFs and the main IMFs' relative motion with respect to the remaining system. This concerns a restricted time interval of about 120 fm/c, during which these fragments arise from the hot intermediate system.

In particular, in Fig. 12(b), for selected events with $A_{HL} < 5$, we have shown the average angle $\overline{\Phi}_{plane}$ as a function of time. The increasing trend is clearly visible, with a characteristic rise time of about 400 fm/c, up to a saturation value near the average values of the theoretical distribution (evaluated at 800 fm/c), which is shown in Fig. 9. For the events selected, $\overline{\Phi}_{plane}(t = 400)$ is only approximately equal to $\int_{t=0}^{t=400} \frac{\overline{J^r(t)}}{I^r(t)} dt$. In fact, even if the rotational dynamics leading to the observed average Φ_{plane} is dominated by the time evolution of the relative motion (radial and rotational) of the PLF, the TLF, and the third-biggest fragment, it is not possible to find simple and general expressions relating $\overline{\Phi}_{plane}$ with the characteristic dynamical variables of the process. This last point, together with a simple approximation scheme, which in concrete cases should correspond to a restrictive selection of events, is briefly discussed in the Appendix. The same section also describes how this approximation scheme could allow us to directly link the measured $\overline{\Phi}_{plane}$ to the average dynamics governing the angular momentum transfer and fission processes. Finally, we can say that dedicated studies should also be carried out to understand how dynamical effects can affect, in this energy region, the out-of-plane distribution. This aspect is relevant, in fact, from this distribution, and an estimation of the pre-fission PLF spin is usually performed in the hypothesis of a statistical decay.

V. CONCLUSIONS

In this work we have discussed different aspects of a study performed on experimental results obtained for the ^{124}Sn+^{64}Ni system at 35 MeV/nucleon using the forward part of the CHIMERA detector. In particular, a comparison with CoMD-II calculations of the observed multi-breakup processes has been discussed. This comparison shows a substantial agreement with the time scales and reaction mechanisms of ternary events discussed in Ref. [14] related to the "neck" emission. Moreover, a longer characteristic time on the order of 450 fm/c is predicted for the dynamical process that includes a primary binary breakup and a subsequent PLF fission [15]. The model also predicts, on the same time scale in which the "neck" develops, the existence of a more complex dynamical process in which the TLF breaks into at least three fragments and a PLF still survives. Some results of an analysis devoted to highlighting the existence of events that have a structure that is compatible with these dynamical and more complex mechanisms have been presented. The calculations indicate that this mechanism is characterized by prominent nonequilibrium effects in the excitation energy sharing between the two primary sources. Moreover, the calculations suggest that, at a microscopic level, this TLF multi-breakup process is triggered by the transfer of nucleons between PLF and TLF leading to low-density instability of the quasi-target. This process can be considered as a prototype of a fully dynamical induced multi-fragmentation mechanism of nuclei in which the heavy partner mean field plays a dominant role. Further investigations on this subject need to be carried out in the next future. Finally, the rotational dynamics of processes leading to dynamical fission of the heavy partner has been described in the framework of the CoMD-II model. The calculation shows that the average alignment observed can still be understood in terms of the relative rotation between the forming PLF and IMF and therefore through essential collective rotational dynamics. However, the results also show that the overlap in time of processes related to the transfer of angular to the splitting nucleus and to the dynamical fission itself has to be properly taken into account. We note in closing that the resulting possibility of describing both the existence of dynamical processes evolving with different characteristic times and the rotational dynamics leading to PLF fission is largely due to the novel constraint introduced in the CoMD-II approach concerning the conservation rule of the total angular momentum.

ACKNOWLEDGMENTS

Thanks are owed to C. Marchetta and E. Costa for preparing high-quality targets and also to D. Rifuggiato, L. Calabretta, and their co-workers for delivering beams of perfect time characteristics. Finally, we thank also Dr. M. O'Hara for a careful revision of the text.

APPENDIX: ENSEMBLE- AND TIME-AVERAGED ANGULAR VELOCITY

As we have discussed at the end of Sec.IV, the relative motion of the TLF, PLF, and mid-rapidity IMF dominates the average dynamics related to the dynamical fission processes. By assuming that the entrance reaction plane α (determined by the impact parameter and the beam directions) and the experimental one β (determined by the beam and the separation axes directions) are coincident, we obtain the following expressions for the Φ_{plane}, valid at each time for a generic event:

$$\Phi_{plane}(t) = A\arccos\left[\frac{\omega_f R_f C + v_f D}{\left(\omega_f^2 R_f^2 + v_f\right)^{1/2}}\right] - B\arccos\left[\frac{\omega_s R_s \sin(\varphi_s) + v_s \cos(\varphi_s)}{\left(\omega_s^2 R_s^2 + v_s^2\right)^{1/2}}\right], \quad \text{(A1)}$$

$$A = \frac{v_{xf}}{|v_{xf}|}; \quad B = \frac{v_{xs}}{|v_{xs}|}, \quad \text{(A2)}$$

$$C = \cos(\chi)\cos(\varphi_f); \quad D = [1 - \cos(\chi)^2 \cos(\varphi_f)^2]^{1/2}. \quad \text{(A3)}$$

Equation (A1) is obtained by decomposing the relative velocities into angular and radial components. To obtain this expression we have also supposed that the separation and

fission axes do not perform multiple rounds. This condition is supported by CoMD-II calculations for events producing an asymptotic $\Phi_{\rm plane}$ value near the average one [see Fig. 11(b)].

The parameters ω_p, R_p, v_p, and φ_p are referred to the binary systems formed by the TLF and the splitting pre-fissioning PLF ($p = s$) and the one related to the fission products ($p = f$). They are, respectively, the angular velocities, the relative distances, the radial velocities, and the angles of the relative distance vectors with respect to the beam axis. The angle χ represents the angle between the plane α and the plane determined by the fission decay. The term v_{xp} indicates the component of the relative velocities along the impact parameter direction. In deriving these relations we have assumed the following limitations: $0 \leqslant \chi \leqslant \pi/2$ and $0 \leqslant \varphi_p \leqslant \pi$.

At this point, we want to state that these relations and the following considerations are based on a semiclassical picture of the investigated processes. This is consistent with the character of the CoMD-II calculations and it is justified by the high values of the involved angular momenta.

All the introduced quantities in Eqs. (A1)–(A3) are time-dependent variables that need to be evaluated through the dynamics of a generic event. Moreover, we note that Eq. (A1) is not linear; therefore $\overline{\Phi_{\rm plane}(t)}$ evaluated at each time step produces a complicated expression that involves the average value of the aforementioned quantities and their correlation coefficients arising from the fluctuating parts. However, an approximation scheme can be obtained according to the following simplifying hypothesis:

(i) For in-plane multi-breakup processes, $\chi \simeq 0$. With this condition, as is shown by CoMD-II calculations, the events for which the planes α and β are almost coincident (within some degree) are preferentially selected. This selection is stronger than the one that is naturally produced by the mean direction of the total spin and allows a strong reduction in the related fluctuations,

(ii) We suppose an uncorrelated fluctuating motion of the separation axis with respect to the fission one; that is, $\overline{\varphi_f - \varphi_s} = \overline{\varphi_f} - \overline{\varphi_s}$. This is a difficult condition to achieve, because, event after event, the fluctuations of φ_s and φ_p around the respective average values $\overline{\varphi_s}$ and $\overline{\varphi_p}$ are correlated through the underlying dynamics. In concrete cases, to minimize this effect, one can try to further limit the analysis to events for which φ_s changes in a short range compared to the one related to the φ_f variable.

(iii) We can set, for example, $A = B = 1$. However, the sign of the A and B coefficients can be established from the measured $\overline{\varphi_s}$ and $\overline{\Phi_{\rm plane}}$; with these conditions, according to the Eq. (A2) and by taking into account that $\lim_{t\to\infty}\omega_p \propto \frac{1}{R_p^2} = 0$ we obtain

$$\overline{\Phi_{\rm plane}(t \to \infty)} \cong \overline{\varphi_f} - \overline{\varphi_s} = \int_{-\infty}^{\infty} \overline{\omega_f} - \int_{-\infty}^{\infty} \overline{\omega_s} dt = \int_{-\infty}^{\infty} \frac{\overline{J^r(t)}}{I^r(t)} dt - \int_{-\infty}^{\infty} \frac{\overline{J^s(t)}}{I^s(t)} dt, \tag{A4}$$

where J^s and I^s are, respectively, the angular momentum and the relative inertia parameter associated with the binary system composed by the TLF and the quasi-PLF splitting nucleus. J^r and I^r represent, respectively, the relative angular momentum and inertia parameter associated with the fission products. As the calculations show, the values of $\overline{\omega_s}$ and $\overline{\omega_f}$ are smooth functions (within the uncertainty associated with the statistics of simulations) localized in time [see, e.g., Fig. 11(a)].

(iv) To obtain a simple relation to connect time and angular velocity information, a further transformation of Eq. (A4) can be performed by substituting the aforementioned dynamical variables with step functions in time:

$$\overline{\varphi_f} - \overline{\varphi_s} = \left\langle \frac{\overline{J^r(t)}}{I^r(t)} \right\rangle \left(T_f^1 - T_f^0\right) - \left\langle \frac{\overline{J^s(t)}}{I^s(t)} \right\rangle T_s. \tag{A5}$$

In these expressions, the brackets indicate time-averaged quantities evaluated over the indicated average time intervals $T_f^1 - T_f^0$ and T_s. In writing this expression, we have chosen as reference the average time when the PLF and TLF start to overlap. For dynamical fission processes, as CoMD-II calculations suggest (see Fig. 3), $T_s < T_f^1$ and $T_f^0 \leqslant T_s$. The second terms of Eq. (A5) can be measured by detecting the three main fragments. The average time interval $T_f^1 - T_f^0$ can be evaluated by means of the method illustrated in Ref. [14] and/or by using more sophisticated N-body approaches.

Therefore, through the selection criteria previously discussed, the measurement of $\overline{\Phi_{\rm plane}}$ can make possible the evaluation of the quite interesting quantity $\langle\overline{\omega_f}\rangle = \langle\frac{\overline{J^r(t)}}{I^r(t)}\rangle$; in fact, it contains the *ensemble- and time-averaged information related to the coupled dynamics of the angular momentum transfer and fission processes*.

Finally, we observe that, for the reaction described in this section and in Sec. IV, the calculation of $\langle\overline{\omega_f}\rangle$ based on an estimation of the total spin by means of the out-plane distributions, described according to the statistical model, and the usage of an a priori calculation of the relative inertia parameter in the usual "sticking" configuration, could be inadequate.

[1] W. U. Schröder and J. Tōke, in *Nonequilibrium Physics at Short Times Scales*, edited by K. Morawetz (Springer-Verlag, Berlin, Heidelberg, New York, 2004), p. 417.
[2] C. P. Montoya *et al.*, Phys. Rev. Lett. **73**, 3070 (1994).
[3] J. F. Lecolley *et al.*, Phys. Lett. **B354**, 202 (1995).
[4] J. Tōoke *et al.*, Nucl. Phys. **A583**, 519 (1995).

[5] E. Plagnol *et al*., Phys. Rev. C **61**, 014606 (1999).
[6] F. Bocage *et al*., Nucl. Phys. **A676**, 391 (2000).
[7] P. Milazzo *et al*., Phys. Lett. **B509**, 204 (2001); Nucl. Phys. **A756**, 39 (2005).
[8] S. Piantelli *et al*., Phys. Rev. C **74**, 034609 (2006).
[9] B. Borderie, J. Phys. G Nucl. Part. Phys. **28**, R217 (2002).
[10] P. Chomaz, M. Colonna, and J. Randrup, Phys. Rep. **389**, 263 (2004).
[11] A. S. Botvina and I. N. Mishustin, Eur. Phys. J. A **30**, 121 (2006).
[12] M. B. Tsang *et al*., Eur. Phys. J. A **30**, 129 (2006).
[13] A. Pagano *et al*., Nucl. Phys. **A681**, 331 (2001).
[14] E. De Filippo *et al*., Phys. Rev. C **71**, 044602 (2005).
[15] E. De Filippo *et al*., Phys. Rev. C **71**, 064604 (2005).
[16] M. Papa, T. Maruyama, and A. Bonasera, Phys. Rev. C **64**, 024612 (2001).
[17] G. Giuliani and M. Papa, Phys. Rev. C **73**, 031601(R) (2006), and references therein.
[18] S. Ayik and C. Grégoire, Phys. Lett. **B212**, 269 (1988).
[19] Ph. Chomaz, G. F. Burgio, and J. Randrup, Phys. Lett. **B254**, 340 (1991).
[20] J. Aichelin, Phys. Rep. **202**, 233 (1991).
[21] C. Dorso, S. Duarte, and J. Randrup, Phys. Lett. **B188**, 287 (1987).
[22] H. Feldmeier and J. Schnack, Rev. Mod. Phys. **72**, 655 (2000).
[23] A. Ono and H. Horiuchi, Prog. Part. Nucl. Phys. **53**, 501 (2004).
[24] M. Papa, A. Bonasera, and T. Maruyama, in *Exotic Clustering*, Proceedings of 4th Relativistic Ion Study CRIS, Catania (Italy), 12–14 June, 2002, AIP Conf. Proc. No. 644, edited by S. Costa, A. Insolia, and C. Tuve (AIP, Melville, NY, 2002), p. 206.
[25] V. E. Viola, K. Kwiatkowski, and M. Walker, Phys. Rev. C **31**, 1550 (1985).
[26] V. Baran, M. Colonna, and M. Di Toro, Nucl. Phys. **A730**, 329 (2004).
[27] M. Papa, G. Giuliani, and A. Bonasera, J. Comput. Phys. **208**, 403 (2005).
[28] A. A. Stefanini *et al*., Z. Phys. A **351**, 167 (1995), and references therein.
[29] J. Colin *et al*., Phys. Rev. C **67**, 064603 (2003), and references therein.